Paull, C.K., Matsumoto, R., Wallace, P.J., and Dillon, W.P. (Eds.), 2000
Proceedings of the Ocean Drilling Program, Scientific Results, Vol. 164

29. METHANE-DERIVED AUTHIGENIC CARBONATES ASSOCIATED WITH GAS HYDRATE DECOMPOSITION AND FLUID VENTING ABOVE THE BLAKE RIDGE DIAPIR[1]

T.H. Naehr,[2,3] N.M. Rodriguez,[4,5] G. Bohrmann,[3] C.K. Paull,[4,3] R. Botz[6]

ABSTRACT

Authigenic carbonates were recovered from several horizons between 0 and 52 mbsf in sediments that overlay the Blake Ridge Diapir on the Carolina Rise (Ocean Drilling Program [ODP] Site 996). Active chemosynthetic communities at this site are apparently fed by fluid conduits extending beneath a bottom-simulating reflector (BSR). Gas hydrates occur at several depth intervals in these near-surface sediments. The carbonate nodules are composed of rounded to subangular intraclasts and carbonate cemented mussel shell fragments. Electron microprobe and X-ray diffraction (XRD) investigations show that aragonite is the dominant authigenic carbonate. Authigenic aragonite occurs both as microcrystalline, interstitial cement, and as cavity-filling radial fibrous crystals. The $\delta^{13}C$ values of the authigenic aragonite vary between –48.4‰ and –30.5‰ (Peedee belemnite [PDB]), indicating that carbon derived from ^{13}C-depleted methane is incorporated into these carbonates. The $\delta^{13}C$ of pore water ΣCO_2 values are most negative in the upper 10 mbsf, near the sediment/water interface (–38‰ ± 5‰), but noticeably more positive below 25 mbsf (+5‰ ± 6‰). Because carbonates derive their carbon from HCO_3^-, dissimilarities between the $\delta^{13}C$ values of carbonate precipitates recovered from greater than 10 mbsf and $\delta^{13}C$ values of the associated pore fluids suggests that these carbonates formed near the seafloor. Differences of about 1‰ in the oxygen isotopic composition of carbonate precipitates from different depths are possibly related to changes in bottom-water conditions during glacial and interglacial time periods. Measurements of the strontium isotopic composition on 13 carbonate samples show $^{87}Sr/^{86}Sr$ values between 0.709125 and 0.709206 with a mean of 0.709165, consistent with the approximate age of their host sediment. Furthermore, the $^{87}Sr/^{86}Sr$ values of six pore-water samples from Site 996 vary between 0.709130 and 0.709204. The similarity of these values to seawater ($^{87}Sr/^{86}Sr$ = 0.709175), and to $^{87}Sr/^{86}Sr$ values of pore water from similar sample depths elsewhere on the Blake Ridge (Sites 994, 995, and 997), indicates a shallow Sr source. The $^{87}Sr/^{86}Sr$ values of the authigenic carbonates at Site 996 are not consistent with the Sr isotopic values predicted for carbonates precipitated from fluids transported upward along fault conduits extending through the base of the gas hydrate–stability zone. Based on our data, we see no evidence of continuing carbonate diagenesis with depth. Therefore, with the exception of their seafloor expression as carbonate crusts, fossil vent sites will not be preserved. Because these authigenic features apparently form only at the seafloor, their vertical distribution and sediment age imply that seepage has been going on in this area for at least 600,000 yr.

INTRODUCTION

Cold seeps and vents have been found along almost all convergent plate boundaries (e.g., Kulm et al., 1986; Le Pichon et al., 1992; Wallmann et al., 1997) and on many passive continental margins (e.g., Paull et al., 1984; Hovland, 1992; Aharon et al., 1997). Distinctive colonies of clams, tube worms, and precipitates of authigenic minerals mark areas of fluid discharge and are the result of both biogeochemical turnover and the interaction between fluids and ambient bottom water at cold vent sites (Suess et al., 1985; Paull et al., 1992; Roberts and Aharon, 1994; Paull et al., 1995b, Barry et al., 1996). The co-occurrence of gas hydrates and fluid venting at several locations (e.g., the Sea of Okhotsk [Soloviev and Ginsburg, 1997], the Eel River Basin [Brooks et al., 1991], the Cascadia Margin [Carson, Westbrook, Musgrave, Suess, et al., 1995; Sample and Reid, 1998; Bohrmann et al., 1998] and the Blake Ridge [Paull et al., 1995b]) indicates a relationship between gas hydrate decomposition, venting of methane-rich fluids, and the formation of authigenic carbonates at the seafloor.

The chemical environment at most vent sites appears to be controlled by the flux of gases to the seafloor and rates of biologically induced reactions, which affect both the bicarbonate and sulfate activities. Furthermore, chemosynthetic benthic fauna is supported by CH_4- and H_2S-oxidizing and SO_4^{2-}-reducing bacteria. Whereas aerobic oxidation of methane favors calcite dissolution instead of precipitation (Wallmann et al., 1997), the anaerobic oxidation of methane via sulfate reduction generates HCO_3^- and can, therefore, produce oversaturation of pore water with respect to calcite and other carbonate minerals (Reeburgh, 1980):

$$CH_4 + SO_4^{2-} \rightarrow HCO_3^- + HS^- + H_2O. \quad (1)$$

Drilling at the Blake Ridge Diapir vent site (Site 996) during ODP Leg 164 focused on processes related to methane migration and gas hydrate formation/decomposition in a fault zone where methane, presumably derived from gas hydrates below, is leaking out onto the seafloor. Drilling at this site provided the unique opportunity to study the connection between the seafloor phenomena of cold seeps and the reservoir from which these fluids might originate, and how the mineralogical, geochemical, and isotopic composition of mineral precipitates might be affected by the temporal or spacial evolution of fluids within such fault conduits. New mineralogical, chemical, and isotope data from authigenic carbonate precipitates presented in this paper provide a record of active fluid venting above the Blake Ridge Diapir. These results, when compared to data from the associated pore fluids

[1]Paull, C.K., Matsumoto, R., Wallace, P.J., and Dillon, W.P. (Eds.), 2000. *Proc. ODP, Sci. Results,* 164: College Station, TX (Ocean Drilling Program).
[2]GEOMAR Research Center for Marine Geosciences, 24148 Kiel, Federal Republic of Germany.
[3]Present address: Monterey Bay Aquarium Research Institute, 7700 Sandholdt Road, Moss Landing, CA 95039, U.S.A. Correspondence author: tnaehr@mbari.org
[4]Department of Geology, University of North Carolina, Chapel Hill, NC 27599, U.S.A.
[5]Present address: Exxon Exploration Company, P.O. Box 4778, Houston, TX 77210-4778, U.S.A.
[6]Department of Geology and Paleontology, University of Kiel, 24118 Kiel, Federal Republic of Germany.

and gases, provide the means to establish the connection between the fluid reservoir, fluid conduits, and the formation of mineral precipitates.

The carbon isotopic composition of authigenic carbonates serves as an indicator for the origin of carbon incorporated during carbonate precipitation (e.g., Reeburgh, 1980; Anderson and Arthur, 1983; Ritger et al., 1987). Sources of carbon to the pore fluids include (1) biogenic methane ($\delta^{13}C$ <–65‰ PDB) or thermogenic methane ($\delta^{13}C$ –30‰ to –50‰); (2) sedimentary organic carbon ($\delta^{13}C$ ~–25‰); and (3) marine biogenic carbonate or seawater CO_3^{2-} with a $\delta^{13}C$ value near 0‰. Ultimately, the amount of mixing between these different components will determine the $\delta^{13}C$ value of any authigenic carbonate (Paull et al., 1992).

Oxygen isotope ratios, on the other hand, may provide information pertaining to the temperature and origin of fluids from which authigenic carbonates are precipitated. Additionally, zonation patterns of carbon and oxygen isotopes within the carbonate nodules provide insights into changes of the isotopic composition of the pore fluids during the process of cementation.

The objectives of this study are (1) to document and summarize the occurrence and distribution of authigenic carbonates recovered from several depth intervals in sediments above the Blake Ridge Diapir (Site 996); (2) to investigate the petrographic, geochemical and isotopic characteristics of these carbonates; (3) to infer the nature and source of fluids associated with carbonate formation; and (4) to address the question of whether authigenic mineral formation at vent sites is mainly restricted to the seafloor, or if there is ongoing diagenesis with depth. Authigenic carbonates recovered from as deep as 60 mbsf into this active vent site provided us with an unparalleled opportunity to investigate the spatial variability of vent-derived authigenic mineral precipitates.

GEOLOGICAL SETTING

Site 996 is located above the crest of the Blake Ridge Diapir on the northwestern end of the Blake Ridge (Fig. 1). The Blake Ridge is a large Neogene and Quarternary sediment drift deposited by the Western Boundary Undercurrent (WBUC) that consists of hemipelagic silt- and clay-rich contourite deposits (Tucholke and Mountain, 1979). The Blake Ridge Diapir is the southernmost in a linear array of about 20 diapiric structures that rise out of the base of the Carolina Trough from as much as 12 km below sea level (e.g., Dillon et al., 1982). The region around the diapir displays a strong bottom-simulating reflector (BSR; Paull and Dillon, 1981) at an approximate depth of 450 mbsf, but curves upward around the flanks of the diapir. Although the cause of this curvature is unclear, it may be related to changes in gas hydrate stability induced by increased heat or salt around the flanks of the diapir.

Seafloor venting of microbial gases on top of the Blake Ridge Diapir was discovered by Paull et al. (1995b). Acoustically identified, gas-rich plumes extend as much as 320 m above a pockmarked seafloor displaying active chemosynthetic communities. These plumes apparently emanate from a seafloor pockmark that is located above a fault extending down towards a dome in the BSR (Fig. 2). Side-scan sonar data reveal a reflective seafloor along the trace of this fault zone. Photographic surveys and sampling (Paull et al., 1995b) indicate that these reflective patches are associated with biological communities and methane-derived carbonate cements.

Solid gas hydrates were recovered from all holes drilled at Site 996. The presence of gas hydrates near the sediment surface indicates that, at present, gas hydrates are stable under seafloor pressure/temperature (P/T) conditions. Pore-fluid data and the presence of active chemosynthetic communities at Site 996 are indicative of upward vertical transport of methane-rich fluids. The methane content of headspace gases in sediments near the pockmark increases from 1300 to 11,000 ppm with increasing depth to 60 mbsf. Sulfate concentrations approach 0 mM near the seafloor (Paull, Matsumoto, Wallace, et al., 1996). This rapid SO_4^{2-} depletion, together with high concentrations of interstitial CH_4, low amounts of sedimentary organic matter (<0.5%; Paull, Matsumoto, Wallace, et al., 1996), and high levels of dissolved ΣHS^- indicate that anaerobic methane oxidation is occurring at Site 996 (Borowski et al., 1997). Given the low level of sedimentary organic matter, these observations are consistent with advective transport of CH_4, which supports the chemosynthetic community on the seafloor above the Blake Ridge Diapir. Intense microbial oxidation of CH_4 increases alkalinity, thus promoting carbonate precipitation. Sharp decreases in Ca^{2+}, Mg^{2+}, and Sr^{2+} concentrations immediately below the sediment/water interface suggests uptake of these elements into authigenic carbonates (Paull, Matsumoto, Wallace, et al., 1996).

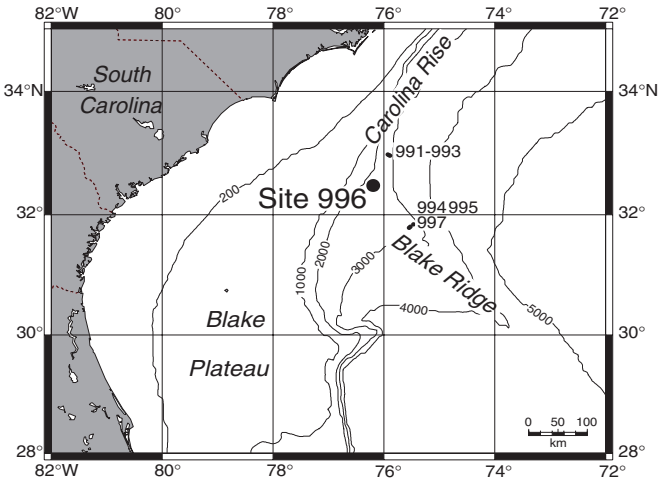

Figure 1. Map of the study area of ODP Leg 164. Site 996 is located on the Blake Ridge directly above the Blake Ridge Diapir. Contours are in meters.

METHODS

Sedimentary Petrography

Textural, compositional, and morphological features of carbonate precipitates were studied and described on hand specimens, slabs, and polished thin sections using light and scanning electron microscopy (CamScan SEM) at the GEOMAR Research Center for Marine Geosciences. The CamScan SEM was equipped with an energy dispersive X-ray spectrographic analyzer (EDAX) that allowed us to obtain qualitative elemental analyses of selected mineral grains.

Carbonate Content and X-ray Diffraction Analysis

Bulk mineralogy and the relative abundance of different carbonate minerals in each sample, were investigated by X-ray diffraction (XRD) using a Philips PW 1820 X-ray diffractometer at the GEOMAR Research Center for Marine Geosciences and a Philips Norelco 1720 X-ray diffractometer at the University of North Carolina at Chapel Hill, both generating monochromatic Cuk_α radiation. Samples were crushed with an agate mortar and pestle, mixed with an internal standard (α-Al_2O_3), and prepared as randomly oriented powder slides. Scans were run from 20° to 60° 2θ at a scanning speed of 0.01° 2θ/s. The relative proportions of different carbonate minerals were quantified on the basis of the (104) peak areas of calcite, Mg-calcite and dolomite, and the (111) peak area of aragonite using prepared calibration curves. For details about the calibration, see Greinert (in press). The position of the (104) peak was used to determine Mg content of carbonate minerals (Goldsmith et al., 1961; Lumsden, 1979). Calcite with less than 5 mol% $MgCO_3$ is considered low-Mg calcite (LMC), and all other calcite compositions are referred to as high-Mg calcite (HMC) after Burton and

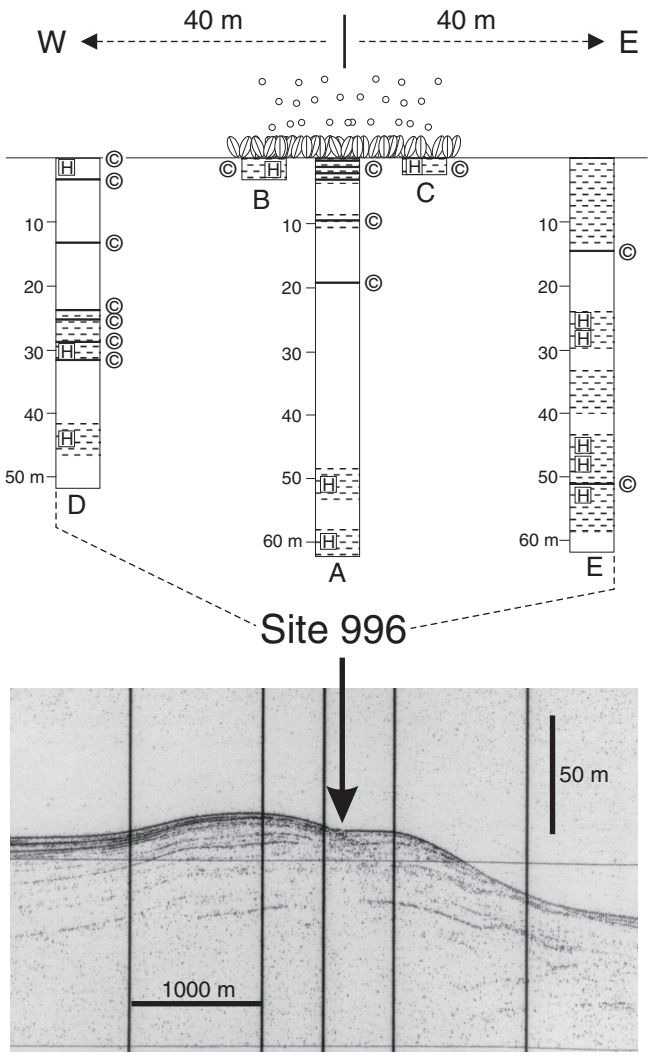

Figure 2. A 3.5-kHz echogram over the Blake Ridge Diapir showing the location of Site 996, which was drilled into a small depression on the crest of the diapir. Graphic logs show lithology for each hole (Holes 996A through 996E). C = carbonate nodule(s); H = gas hydrate occurrences. Intervals of no recovery are blank.

Walter (1987). Carbon and carbonate contents (expressed as weight percent [wt%] $CaCO_3$) of both carbonate precipitates and background sediment samples were determined using a NA-1500 Carlo-Erba element analyzer at the GEOMAR Research Center for Marine Geosciences and a Coulometrics Model 5011 CO_2 Coulometer at the University of North Carolina at Chapel Hill.

Electron Microprobe Analyses

Carbon coated, polished thin sections were made from selected authigenic carbonates and examined by electron microprobe analyses to provide detailed mineral chemistry of carbonate precipitates. All analyses were performed using a Cameca SX 50 electron microprobe at the GEOMAR Research Center for Marine Geosciences, which is equipped with a wavelength dispersive system. During a typical analysis, concentrations of Ca, Mg, Mn, Fe, Sr, Ba, C, O, Al, and P were determined. Counts were collected for 20 s using an accelerating voltage of 15 kV and a beam current of 10 nA in scanning mode (magnification 25,000). Natural carbonate minerals, feldspars, and glasses were used as standards. Matrix corrections were made using standard *ZAF* techniques.

Stable Isotope Analyses

Samples for oxygen and carbon isotope analyses were extracted from the surfaces of polished slabs using a hand-held microdrill. The CO_2 for analysis was obtained by reacting samples with 100% orthophosphoric acid *in vacuo* at 75°C (Carbo Kiel CO_2 preparation device). The purified CO_2 gas was analyzed isotopically in a Finnigan MAT 252 mass spectrometer at the Geological Institute Erlangen. Results are expressed in δ notation relative to the Peedee belemnite (PDB) standard. Precision is on the order of 0.1‰ for both oxygen and carbon. The $\delta^{18}O$ values for dolomite have been corrected following the method proposed by Rosenbaum and Sheppard (1986). Pore-water oxygen isotope data are from Borowski et al. (1997).

Stable oxygen and carbon measurements on bulk sediments were measured on a Finnigan Mat 251 Ratio Mass Spectrometer at the North Carolina State Stable Isotope Laboratory. Samples were roasted under vacuum at 325°C for 1 hr to remove volatile organics and then reacted at 75°C for 10 min with 100% orthophosphoric acid in side-arm reaction vessels. The CO_2 was cryogenically separated for analysis. Because many of these samples contained sulfides, an additional cryogenic separation was done at ~ –130°C to insure that any SO_2 produced during the digestion procedure would be separated from CO_2 (Rodriguez et al., Chap. 30, this volume).

Strontium Isotope Analysis

The $^{87}Sr/^{86}Sr$ composition of 15 carbonate and six pore-water samples was determined using a VG-Sector 54 Thermal Ionization Mass Spectrometer at the Department of Geology, University of North Carolina at Chapel Hill. Samples for $^{87}Sr/^{86}Sr$ analysis were microdrilled adjacent to samples for $\delta^{13}C$ and $\delta^{13}O$ determination. Samples were dissolved in 500-µL 1-M ultra-pure acetic acid, centrifuged, and then the decantate was evaporated dry. Samples were then redissolved in 250 µL of 5-N HNO_3 and loaded into columns containing Eichrom Sr-specific resin. Details of the procedure are given in Paull et al. (1995a). Values of $^{87}Sr/^{86}Sr$ are reported relative to a $^{87}Sr/^{86}Sr$ ratio of 0.71025 for SRM-987. Replicate analyses of SRM indicate uncertainties of ±0.000011 (1σ). For pore-water $^{87}Sr/^{86}Sr$ analyses, see Paull et al. (1995a).

RESULTS

Occurrence and Distribution of Authigenic Carbonates

Authigenic carbonate concretions were recovered from various depths in Holes 996A, 996B, 996C, 996D, and 996E (Fig. 2). Zones of poorest sediment recovery at Site 996 coincided with significant decreases in penetration rates during drilling (Paull, Matsumoto, Wallace, et al., 1996), and material recovered from those zones consisted entirely of fragments of indurated carbonates. Lithified carbonates and background sediment samples analyzed for this study are noted as type "C" and "S," respectively, in Tables 1, 3, and 4. The low recovery and the relatively small size of the samples resulted in a certainly incomplete, but nevertheless unique set of samples from a site of active fluid venting.

Petrography

The carbonate-cemented deposits were classified on the basis of their level of internal brecciation and the size and nature of their intraclasts. Although the distinctive characteristics of the carbonate-cemented deposits overlap, they can be separated into three general types. All carbonate nodules (except for one) are composed predominantly of aragonite (Table 1). In addition, generally fibrous or botryoidal aragonite cements have developed in open pore space, either between intraclasts or inside the cavities of biogenic components such as foraminifers or bivalve shells (Figs. 3A, 4A, 4B). Commonly,

well-developed idiomorphic hexagonal crystals of aragonite incompletely fill the pore spaces.

The first type of nodule (referred to as "type 1"; Fig. 3A) shows a large number of shell fragments and rounded to subangular, micritic intraclasts (5–20 mm in size). The intraclasts consist of carbonate-cemented siltstones and mudstones with micritic cements and often exhibit a distinctly darker color than the surrounding matrix. Foraminifers and bivalve fragments are a dominant biogenic component of the nodules. Clay minerals and silt-sized quartz, feldspar, and glauconite constitute the clastic and noncarbonate components. The matrix also consists of carbonate-cemented siltstones and mudstones with both micritic and sparitic cements; both cements are composed predominately of aragonite. The microcrystalline carbonate grains never exceed 10 µm and are generally ~2 µm in size. The micrite often exhibits a peloidal texture (Fig. 3B) and did not replace detrital grains. Sparitic aragonite cements occur as radial fibrous and radiating bladed aragonite crystals and fill open pore space between intraclasts. Elongate radiating aragonite crystals are up to 0.55 mm long. Both disseminated and framboidal pyrite is common, frequently filling foraminifer tests (Fig. 3F).

A second type ("type 2") of carbonate precipitate (Fig. 3C) is similar in composition and fabric to type 1 precipitates, but contains fewer intraclasts and more shell debris. The bivalve shells are broken into small pieces (< 1 cm), so that the carbonates have the appearance of cemented shell hash (Fig. 3C). The micritic matrix displays lighter and darker areas, apparently due to differences in carbonate content.

Table 1. Carbonate mineralogy of Site 996 sediments and carbonate precipitates based upon carbonate content determination and X-ray diffraction analyses.

Core, section, interval (cm)	Depth (mbsf)	Type	Relative percentages (wt%)				Mole% Mg (%)		$CaCO_3$ corrected (wt%)			
			Calcite	Aragonite	Mg-calcite	Dolomite	In Mg-calcite	In dolomite	$CaCO_3$	Calcite	Mg-calcite	Aragonite
164-996A-												
1H-1, 4-6	0.04	C	3	97	—	—			87.0	3		84
1H-1, 4-6	0.04	S	4	96	—	—						
1H-1, 21-23	0.21	C	4	96	—	—			76.0	3		73
1H-1, 21-23	0.21	S	3	97	—	—						
1H-1, 32-34	0.32	C	2	98	—	—			88.8	2		87
1H-1, 32-34	0.32	S	3	97	—	—						
1H-1, 52-54	0.52	C	3	97	—	—			84.4	3		82
1H-1, 52-54	0.52	S	2	98	—	—						
1H-1, 63-65	0.63	C	3	96	1	—	12		77.8	2	1	75
1H-1, 63-65	0.63	S	4	95	1	—	13					
1H-1, 72-74	0.72	C	3	93	3	1	14	50	70.7	2	2	66
1H-1, 72-74	0.72	S	10	87	3	—	15					
1H-1, 85-95	0.85	C	2	95	3	—	ND		79.0	2	2	75
1H-1, 85-95	0.85	S	14	84	2	—	ND		54.0	8	1	45
1H-2, 15-16	1.05	C	3	96	1	—	13		73.7	2	1	71
1H-2, 15-16	1.05	S	33	67	—	—						
1H-2, 39-41	1.29	C	4	95	1	—	11		71.0	3	1	67
1H-2, 39-41	1.29	S	27	73	—	—						
1H-2, 56-58	1.46	C	4	95	1	—	14		79.1	3	1	75
1H-2, 56-58	1.46	S	21	73	6	—	14					
1H-4, 35-36	2.70	S	30	54	16	—	9					
1H-5, 44-46	3.23	S	49	51	—	—						
1H-6, 33-38	3.62	S	59	37	4	—	ND		50.0	30	2	19
2H-1, 34-36	8.84	S	48	52	—	—						
2H-CC, 14-16	9.13	C	14	79	7	—	11		65.5	9	5	52
2H-CC, 14-16	9.13	S	26	68	6	—	11					
3X-1, 34-36	9.84	S	57	43	—	—						
3X-1, 50-52	10.00	C	10	84	6	—	11		76.2	8	5	64
3X-1, 61-71	10.11	S	62	30	8	—	ND		34.0	21	3	10
8H-1, 35-37	48.85	S	47	53	—	—						
8H-2, 0-12	49.61	S	76	—	24	—	ND		13.0	10	3	
8H-3, 35-37	50.18	S	67	—	33	—	14					
9H-1, 35-37	58.35	S	42	58	—	—						
9H-3, 35-37	61.03	S	42	58	—	—						
9H-3, 87-102	61.55	S	69	31	—	—			27.0	19		8
164-996B-												
1H-1, 0-5	0.00	C	3	95	2	—	11		72.0	2	1	68
1H-1, 0-5	0.00	C	4	96	—	—			83.5	3		80
1H-1, 5-7	0.05	C	3	93	4	—	14		80.0	2	3	74
1H-1, 5-7	0.05	S	6	94	—	—						
1H-1, 35-37	0.35	C	7	93	—	—						
1H-1, 35-37	0.35	S	11	86	3	—	14					
1H-1, 37-39	0.37	C	4	93	2	1	13	50	67.7	3	1	63
1H-1, 37-39	0.37	S	10	87	3	—	13					
1H-1, 85-87	0.85	C	4	93	2	1	14	51	66.4	3	1	62
1H-1, 85-87	0.85	S	11	86	3	—	13					
1H-2, 60-62	1.52	S	18	72	10	—	10					
1H-3, 52-54	2.49	S	33	60	7	—	13					
1H-3, 135-150	2.44	S	55	39	6	—	ND		47.0	26	3	18
1H-4, 35-37	2.94	S	44	35	21	—	10					
1H-4, 47-49	3.06	S	54	46	—	—						
164-996C-												
1H-1, 51-53	0.51	C	—	100	—	—			95.4			95
1H-1, 51-53	0.51	S	8	92	—	—						
1H-1, 56-58	0.56	C	4	96	—	—			91.9	4		88
1H-1, 56-58	0.56	S	6	94	—	—						
1H-1, 63-65	0.63	C	1	99	—	—			91.8	1		91
1H-1, 63-65	0.63	S	4	96	—	—						
1H-1, 70-72	0.70	C	4	96	—	—			86.2	3		83
1H-1, 108-114	1.08	C	3	93	4	—	ND		75.0	2	3	70
1H-1, 108-114	1.08	S	29	66	5	—	ND		42.0	12	2	28
1H-2, 67-77	1.81	C	14	77	9	—	ND		61.0	9	5	47
1H-2, 67-77	1.81	S	37	49	14	—	ND		36.0	13	5	18

Table 1 (continued).

Core, section, interval (cm)	Depth (mbsf)	Type	Relative percentages (wt%)				Mole% Mg (%)		$CaCO_3$ corrected (wt%)			
			Calcite	Aragonite	Mg-calcite	Dolomite	In Mg-calcite	In dolomite	$CaCO_3$	Calcite	Mg-calcite	Aragonite
1H-3, 2-4	1.93	S	32	56	12	—	13					
1H-3, 29-31	2.20	C	3	95	2	—	14		72.8	2	1	69
2H-CC, 0-2	2.40	C	11	78	11	—	11		58.2	6	6	45
2H-CC, 0-2	2.40	S	21	72	7	—	13					
2H-CC, 3-5	2.43	C	14	76	9	1	9	55	77.6	11	7	59
2H-CC, 3-5	2.43	S	21	76	3	—	14					
164-996D-												
1H-CC, 0-20	0.00	S	34	65	1	—	ND		59.0	20	1	38
1H-CC, 20-40	0.20	C	5	95	—	—			90.0	5		86
1H-CC, 20-40	0.20	S	20	79	1	—	ND		60.0	12	1	47
3X-CC, 9-11	13.09	C	5	93	2	—	10		83.4	4	2	78
4H-1, 12-14	22.72	S	100	-	—	—						
4H-6, 101-103	28.25	S	54	46	—	—						
4H-6, 135-150	28.59	S	48	48	4	—	ND		28.0	13	1	13
5X-CC, 7-9	32.17	C	5	95	—	—			77.2	4		73
5X-CC, 23-25	32.33	C	4	94	2	—	10		80.1	3	2	75
6H-2, 10-12	42.57	S	57	43	—	—						
6H-2, 52-67	42.99	S	57	43	—	—			28.0	16		12
6H-6, 35-37	46.71	S	48	52	—	—						
164-996E-												
1H-1, 35-37	0.35	S	34	66	—	—						
1H-3, 35-37	3.35	S	46	54	—	—						
1H-3, 72-87	3.72	S	57	34	—	—			49.0	28		17
2H-1, 34-36	4.44	S	45	55	—	—						
2H-1, 137-144	5.45	S	44	51	5	—	ND		29.0	13	1	15
2H-1, 144-150	5.52	S	92	—	8	—	ND		26.0	24	2	
2H-2, 135-150	6.95	S	65	32	3	—	ND		58.0	38	2	19
2H-3, 35-37	7.45	S	54	46	—	—						
2H-4, 134-150	9.94	S	94	—	6	—	ND		28.0	26	2	
3X-CC, 0-7	13.60	C	8	92	—	—			96.5	8		89
3X-CC, 8-12	13.68	C	14	86	—	—			88.7	12		76
3X-CC, 21-25	13.81	C	12	88	—	—			79.9	10		70
4H-4, 35-37	27.25	S	46	54	—	—						
4H-5, 135-150	29.05	S	99	—	1	—	ND		30.0	30		
5H-2, 35-37	33.38	S	83	—	17	—	13					
5H-4, 35-37	35.90	S	46	54	—	—						
6X-6, 135-150	50.86	S	97	—	3	—	ND		33.0	32	1	
6X-CC, 11-13	51.62	C	11	—	—	89		45	82.6	9	74*	

Notes: S = sediment, C = carbonate nodule. * = dolomite. — = below detection limit. ND = not determined.

Voids between intraclasts and bivalve shells are completely or partially filled with fibrous or bladed aragonite, often showing multiple stages of mineral growth (Fig. 3D). Well-developed radiating crystals of aragonite occur where large pore spaces exist (Figs. 4A, 4B).

Finally, a third type of authigenic carbonate ("type 3") has no, or only very few, intraclasts. Fibrous aragonite cements are not developed. As in types 1 and 2, silt-sized quartz, feldspar, glauconite, clay minerals, and foraminifers are the main detrital components. Pyrite is common. Aragonite occurs exclusively as microcrystalline cement, filling the pore space between the detrital sediment grains. Many samples, as well as some of the larger intraclasts, show a distinctly darker rim surrounding a lighter core (Fig. 3E). One carbonate nodule recovered from 51.6 mbsf (Hole 996E) has a similar fabric, but is cemented by dolomite and not aragonite.

Mineralogy

The carbonate content of the cemented sediments ranges from 58.3 wt% to 96.5 wt% $CaCO_3$ with a mean of 79.7 wt% (Table 1), which is significantly higher than the mean $CaCO_3$ value of background sediment (~35 wt%; Paull, Matsumoto, Wallace, et al., 1996). Based on these data, we infer that the nodules contain 23–63 wt% carbonate cement. Furthermore, aragonite is more abundant in the carbonate nodules than in the surrounding sediment, confirming the petrographic observation that aragonite is the predominating authigenic mineral at Site 996 (Fig. 5). High-Mg calcite (HMC) only occurs in minor amounts (<10%) and may be detrital in origin. Magnesium content ranges between 9 and 14 mol% $MgCO_3$. The only exception is Sample 164-996E-6X-CC, 11–13 cm, which is a dolomite nodule with 45 mol% $MgCO_3$ (Table 1).

Electron microprobe analyses of pure aragonite cements show Sr contents ranging from 5300 to 11,900 ppm (Table 2). Contents of Mg, Mn, and Fe remain below 0.1 wt%. No regular compositional zoning was recognized across the carbonate nodules.

Isotopic Composition of the Carbonates

Stable isotopes of carbon and oxygen were measured on 56 bulk samples (including both carbonate nodules and background sediment) and on 55 individually microdrilled samples from carbonate-cemented matrix, pure aragonitic cements, and from bivalve shells (Tables 3, 4). The $\delta^{18}O$ values of bulk carbonate and sediment samples ranges between 0.2‰ and 4.6‰, representing both biogenic (foraminifers and bivalve shells) and authigenic carbonate (Fig. 6). Samples of cemented matrix and pure aragonite cements have $\delta^{18}O$ values that vary between 3.3‰ and 4.9‰ with a mean of 3.9‰ (Table 3). The $\delta^{13}C$ composition of nodules ranges from –30.5‰ to –48.4‰, and $\delta^{13}C$ values of bulk sediments vary between –0.3‰ and –33.4‰. The dolomite nodule from Hole 996E is unique in that it shows $\delta^{13}C$ and $\delta^{18}O$ values of –13.1‰ and –19.2‰ and 4.8‰ and 5.4‰, respectively.

The $^{87}Sr/^{86}Sr$ isotopic composition of 13 microdrilled carbonate samples, three bivalve shells, and six pore-water samples was measured from this site. The $^{87}Sr/^{86}Sr$ values of nine pore-water samples taken from the upper 65 m at Sites 994, 995, and 997 are reported as well (Table 4). The $^{87}Sr/^{86}Sr$ values of the 13 aragonite samples range between 0.709125 and 0.709206 with a mean of 0.709165. The three bivalve shells have a Sr isotopic composition of 0.709085, 0.709141, and 0.709173, respectively. The pore-water $^{87}Sr/^{86}Sr$ values vary between 0.709130 and 0.709204. All Sr isotope data are plotted against

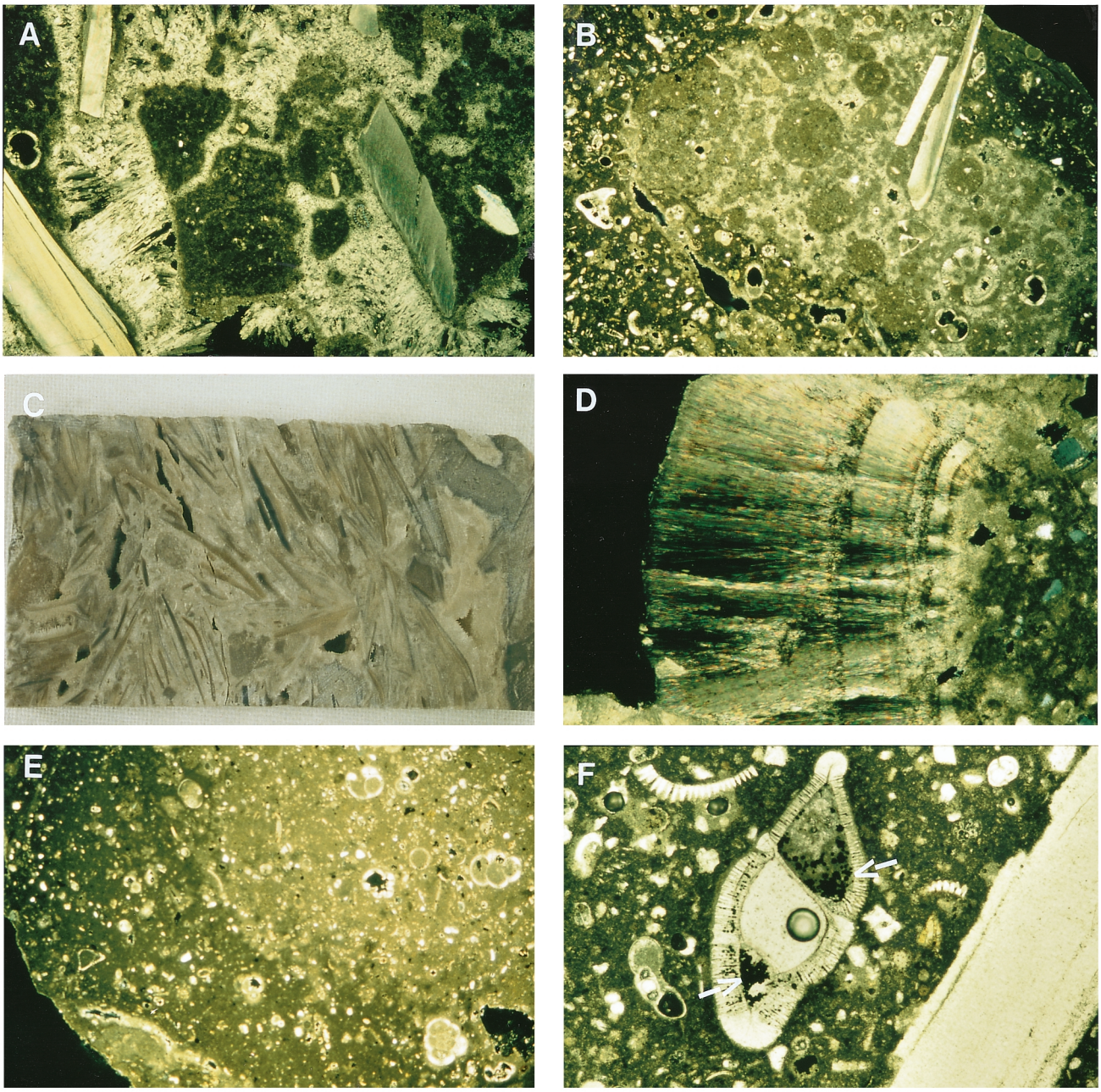

Figure 3. Photomicrographs of Site 996 samples. **A.** Sample 164-996D-5X-CC, 23–25 cm, represents carbonate precipitates of "type 1." Shell fragments and intraclasts, together with void-filling botryoidal aragonite cements are shown. Cross-polarized light; length of view 5.4 mm. **B.** Sample 164-996D-3X-CC, 9–11 cm, is a micritic carbonate nodule with peloidal texture. Cross-polarized light; length of view 5.4 mm. **C.** Sample 164-996E-3X-CC, 0–7 cm. Carbonate precipitate of "type 2." Length of view 5 cm. **D.** Sample 164-996E-3X-CC, 12–15 cm. Botryoidal aragonite shows multiple stages of mineral growth (dark bands parallel to growth direction). Plane-polarized light; length of view 1.3 mm. **E.** Sample 164-996B-1H-01, 0–5 cm. Micritic carbonate nodule of "type 3" with a distinctly darker rim surrounding a lighter colored core. Cross-polarized light; length of view 5.4 mm. **F.** Sample 164-996D-3X-CC, 9–11 cm. Authigenic, framboidal pyrite (arrows) occurs as infilling of a foraminifer test. Plane-polarized light; length of view 1.3 mm.

depth (Fig. 7) and are shown relative to the Sr isotopic reference curve for Neogene seawater after Farrell et al. (1995) and the mean $^{87}Sr/^{86}Sr$ ratio of pore water at the BSR (~450 mbsf) in Sites 994, 995, and 997.

DISCUSSION

Precipitation of Carbonates

Mixing of sulfate- and methane-bearing fluids is occurring at Site 996 (Paull, Matsumoto, Wallace, et al., 1996) and other vent locations (Suess and Whiticar, 1989; Borowski et al., 1996; Wallmann et al., 1997). Sulfate gradients with sulfate concentrations approaching 0 mM near the seafloor (0.10–6.95 mbsf; Paull, Matsumoto, Wallace, et al., 1996) suggest that sulfate depletion is driven by methane flux from below (Borowski et al., 1996) and that anaerobic methane oxidation is the principal sulfate-consuming process at Site 996. The upward methane flux, which is required to sustain these reactions above the Blake Ridge Diapir, is most likely occurring along fluid conduits that were observed in seismic reflection data and in the form of vertical, gas hydrate–cemented veins in the sedimentary section.

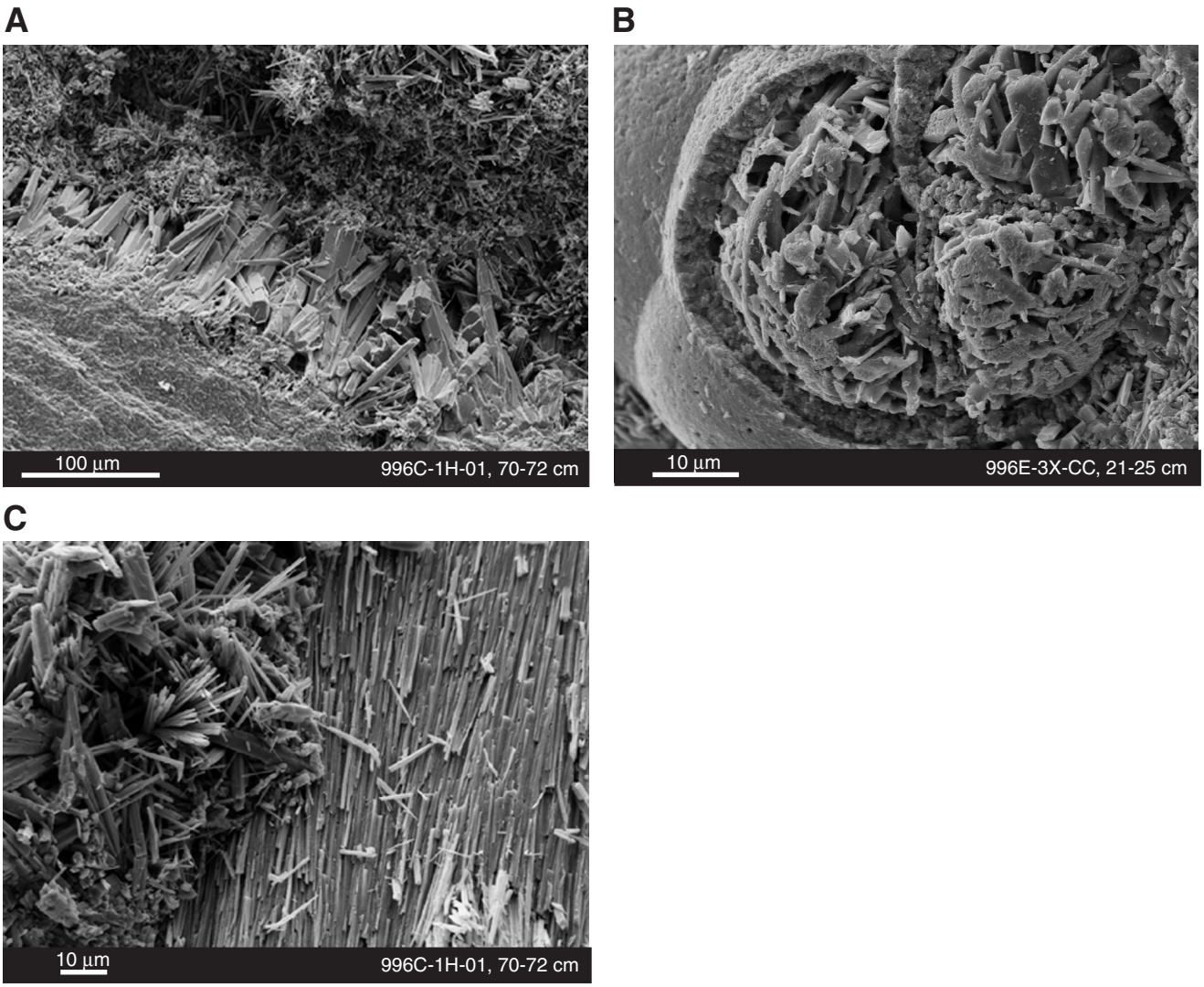

Figure 4. SEM pictures of Site 996 samples. **A.** Authigenic aragonite needles fill the pore space between two intraclasts. **B.** Authigenic aragonite as pore-filling cement inside a foraminfer test. **C.** Corroded surface of a bivalve shell (right) and authigenic aragonite needles (left).

The authigenic carbonate cements at Site 996 are primarily composed of aragonite (Table 1; Fig. 5), which is consistent with authigenic aragonite formation at other vent sites (e.g., Hovland et al., 1987; Matsumoto, 1990; Jørgensen, 1992; Savard et al., 1996). Temperature, the degree of pore-fluid supersaturation, and the presence of oxic or anoxic conditions seem to be the major controlling factors for the precipitation of different carbonate minerals (Burton and Walter, 1987; Hovland et al., 1987; Burton, 1993). The relative importance of those mechanisms, however, is still poorly understood. Elevated temperatures generally seem to favor aragonite precipitation, whereas changes in saturation state seem to have little effect. There have been no definitive means (petrographic, isotopic, or geochemical) for distinguishing between carbonate cements formed under oxic or anoxic conditions. Although aragonite formation has generally been associated with oxic environments at or near the seafloor (Longman, 1980; Hovland et al., 1987, Matsumoto, 1990), the co-occurrence of aragonite and authigenic pyrite in almost all Site 996 samples (Fig. 3F) is difficult to reconcile with oxic conditions, because pyrite can only form in anoxic, sulfate-reducing environments. Thus, the aragonite cements at Site 996 must have formed very near the sediment/water interface in an oxygen-depleted environment where the generation of HCO_3^- by anaerobic methane oxidation resulted in oversaturation with respect to aragonite.

The darker rims on many of the intraclasts may be dissolution rinds that contain less $CaCO_3$. The interaction of sulfide-rich pore fluids with oxygenated seawater ($HS^- + 2O_2 \rightarrow SO_4^{-2} + H^+$) produces locally acidic water (Paull and Neumann, 1987), generating dissolution in carbonates at the sediment/water interface. The rough and partially dissolved surfaces of aragonitic bivalve shells also indicate exposure (either syn- or postdepositionally) to a locally corrosive environment at the seafloor (Fig. 4C). The complex juxtaposition of dissolution surfaces with cemented sediment suggests that the position of the oxic-anoxic interface may fluctuate over time, perhaps in response to variations in the flux of methane from below.

Controls on the Geochemical and Isotopic Composition of the Authigenic Carbonates

The depletion in ^{13}C of the authigenic carbonates at Site 996 ($\delta^{13}C$ as low as –48‰) indicates that CO_2 derived from methane oxidation was the primary carbon source for these carbonates. Based on methane $\delta^{13}C$ values of –62‰ to –72‰ at Site 996 (Paull et al., Chap. 7, this volume), we estimate that up to 75% of the carbon incorporated into authigenic carbonates at this site was derived from biogenic methane.

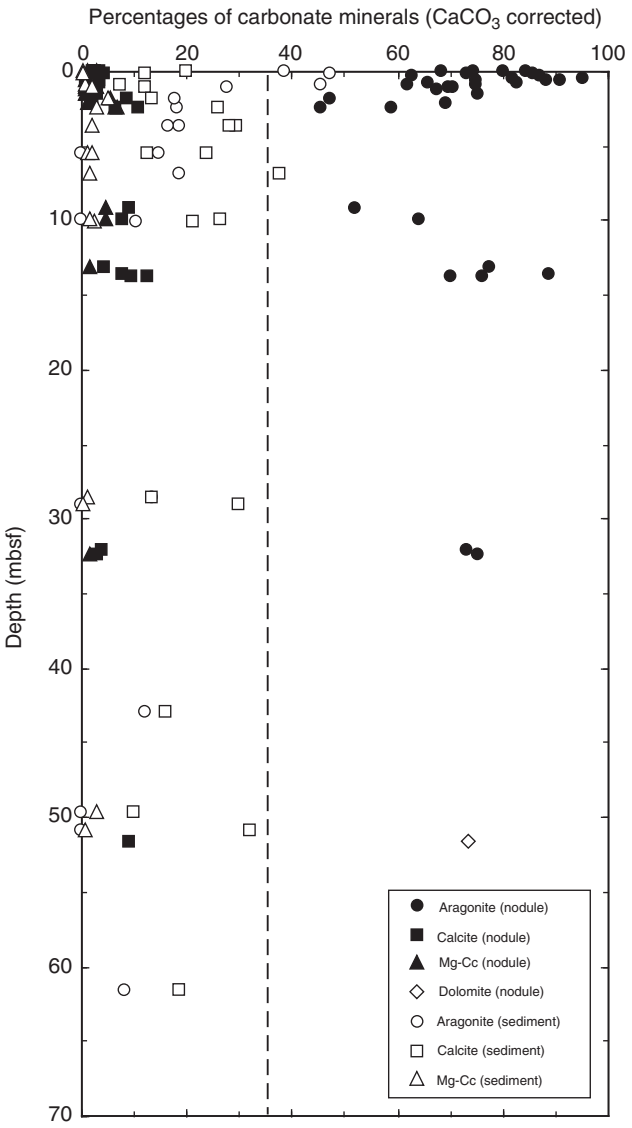

Figure 5. Occurrence and distribution of different carbonate minerals in sediments and carbonate precipitates at Site 996. Carbonate precipitates show clearly elevated aragonite contents. The dashed line represents average carbonate contents (35 wt%) of sediments in this area.

Measurements of the oxygen isotopic composition of pore water of near surface sediments above the Blake Ridge Diapir revealed $\delta^{18}O$ values of 0.1‰ to 0.9‰ with a mean of 0.3‰ (Borowski et al., 1997). Using the $\delta^{18}O_{aragonite}/T$ relationship established by Hudson and Anderson (1989), the $\delta^{18}O$ values of the aragonite cements indicate a precipitation temperature of about 4°C. This is in good agreement with the observed bottom-water temperature of 3.5°C at Site 996 (Paull, Matsumoto, Wallace, et al., 1996). It is therefore reasonable to infer that these cements precipitated in, or near, isotopic equilibrium with the regional bottom water.

Carbon Isotopic Composition of Pore Fluids and Authigenic Carbonates

The carbon isotopic composition of ΣCO_2 in near-surface sediments at Site 996 varies between –28‰ and –45‰ (Paull et al., Chap. 7, this volume). Such negative $\delta^{13}C$ values are typical for concurrent microbial-mediated oxidation of sedimentary organic matter and methane originating from depth (Suess and Whiticar, 1989). As indicated by $\delta^{13}C$ values of –62‰ to –72‰, methane that is consumed at Site 996 is predominately biogenic in origin (Paull et al., Chap. 7, this volume). As authigenic carbonates derive their carbon from the pore-water ΣCO_2 pool (Suess and Whiticar, 1989), the similarity between the $\delta^{13}C$ values of the carbonates (–30.5‰ to –48.4‰) throughout the sedimentary section and pore-water ΣCO_2 (–28‰ to –45‰) at shallow depth indicates that the carbonates have formed from this shallow CO_2 pool. Furthermore, carbon isotope values of ΣCO_2 at Site 996 are most negative near the sediment/water interface and become more positive with depth (Fig. 8). The $\delta^{13}C$ values of recovered authigenic carbonates, however, do not show such a trend (Fig. 9). This dissimilarity again suggests that carbonate nodules recovered from greater depth probably formed near the seafloor, from a ^{13}C-depleted carbon pool similar to the one that currently exists.

There are also indications that the carbon isotopic composition of the ΣCO_2 pool at any one spot changes over time. An isotopic profile of $\delta^{13}C$ values across an aragonite-cemented vein within one of the carbonate nodules (Fig. 10) shows a symmetric trend towards more ^{13}C-depleted carbon isotope values from the rim to the center of the vein. This trend can be explained as the result of a shift in the methane pool from less ^{13}C-depleted to strongly ^{13}C-depleted methane, possibly in response to changes in flow rate (Suess and Whiticar, 1989) or recycling of light carbon in the shallow methanogenic zone (Borowski et al., 1997). Alternatively, this may reflect local changes in the relative importance of the different carbon sources to the pore fluids.

Oxygen Isotopic Variations

As a first approximation, $\delta^{18}O$ values of the carbonate nodules indicate that they precipitated in or near isotopic equilibrium with the regional bottom water. Closer inspection, however, shows that the oxygen isotopic composition of carbonates recovered from shallow depth (0–3 mbsf) differs from those recovered from deeper in the sediment (Figs. 6, 9). This difference in the oxygen isotopic composition is roughly 1‰ (Fig. 6). Although currently highly speculative, this difference in $\delta^{18}O$ might be related to changes in bottom-water conditions, corresponding to glacial and interglacial time periods. However, the relatively poor depth and age control on the carbonate precipitates does not allow a detailed comparison to established Pleistocene $\delta^{18}O$ records.

Strontium Isotope Ratios

Secular variations in the strontium isotopic composition of seawater are well known (e.g., Elderfield, 1986; Farrell et al., 1995). The strontium isotopic composition of carbonate minerals will reflect the strontium isotopic composition of the water in which they formed (Hess et al., 1986). Thus, strontium isotopes can be used to constrain the source of fluids for authigenic carbonate precipitation in marine sediments (Sample and Reid, 1998). To evaluate the source of fluids at this site, we compared the $^{87}Sr/^{86}Sr$ values of authigenic carbonates to the $^{87}Sr/^{86}Sr$ values of pore fluids in nearby sedimentary sections not influenced by venting fluids (Sites 994, 995, and 997).

Because all of the samples that were recovered from Site 996 are Pleistocene in age (Paull, Matsumoto, Wallace, et al., 1996), only a nominal variation in the Sr isotopic composition of the authigenic carbonates is to be expected if the carbonates have formed at or near the seafloor in contact with Pleistocene bottom waters. If, however, there has been addition of strontium from depth, one would expect a different Sr isotopic composition because pore waters from greater depth are known to vary in this area. At Sites 994, 995, and 997 on the Blake Ridge, the Sr isotopic composition at and below the base of gas hydrate stability ranges from 0.709006 to 0.709043 (Fig. 7). If the source of the Sr captured in the authigenic carbonates was being car-

Table 2. Results of electron microprobe analyses on samples 996D-5X-CC, 19–20 cm and 996D-5X-CC, 20–21 cm.

Analysis no.	Weight %											Mole %					
	Ca	Mg	Mn	Fe	Sr	Ba	O	C	Al	P	Total	Ca	Mg	Mn	Fe	Sr	Ba
164-996D-5X-CC, 19-20 cm:																	
3	38.64	—	0.03	—	0.59	—	45.21	14.78	—	0.12	99.36	0.99	—	—	—	0.01	—
4	37.73	0.03	—	0.04	1.01	0.22	43.71	15.50	0.01	0.16	98.40	0.98	—	—	—	0.02	—
5	36.79	0.01	0.03	0.02	0.82	—	42.56	14.98	—	0.13	95.33	0.98	—	—	—	0.01	—
7	38.76	0.02	0.07	0.04	0.89	—	43.86	14.82	—	0.14	98.60	0.98	—	—	—	0.02	—
8	38.37	0.02	—	—	1.19	—	43.55	12.11	0.01	0.14	95.39	0.98	—	—	—	0.02	—
9	38.35	0.01	0.01	0.08	0.83	0.15	42.77	14.45	0.01	0.11	96.77	0.98	—	—	—	0.01	—
11	38.80	—	—	—	0.64	0.20	42.19	13.74	0.01	0.15	95.73	0.99	—	—	—	0.01	—
18	38.31	0.02	—	—	1.09	—	43.73	14.23	0.01	0.14	97.52	0.98	—	—	—	0.02	—
19	38.46	0.03	—	0.05	0.89	0.17	43.69	13.41	—	0.16	96.87	0.98	—	—	—	0.02	—
21	38.15	0.02	—	0.05	0.74	—	43.95	13.07	—	0.13	96.11	0.99	—	—	—	0.01	—
22	37.91	0.02	—	0.04	0.86	0.17	43.88	12.71	—	0.10	95.69	0.98	—	—	—	0.02	—
23	38.09	0.02	0.03	—	0.88	0.20	44.27	14.63	—	0.11	98.23	0.98	—	—	—	0.02	—
24	37.89	0.02	0.07	0.01	0.94	—	44.51	15.27	—	0.15	98.86	0.98	—	—	—	0.02	—
25	37.77	0.02	0.04	0.07	0.65	0.08	45.83	14.20	0.01	0.13	98.80	0.98	—	—	—	0.01	—
26	37.54	0.03	0.01	0.04	1.16	0.03	43.75	13.30	0.01	0.12	95.97	0.98	—	—	—	0.02	—
29	37.74	0.03	—	—	1.09	0.25	43.52	14.28	—	0.14	97.05	0.98	—	—	—	0.02	—
30	37.25	0.02	0.04	—	1.01	—	44.52	16.98	—	0.13	99.95	0.98	—	—	—	0.02	—
33	37.41	0.02	0.03	—	0.91	0.08	44.41	14.90	—	0.12	97.86	0.98	—	—	—	0.02	—
34	36.34	0.02	0.04	—	0.89	—	43.16	18.84	0.01	0.11	99.41	0.98	—	—	—	0.02	—
35	37.83	0.05	0.01	—	0.56	0.18	44.78	14.61	—	0.13	98.14	0.99	—	—	—	0.01	—
36	38.47	0.02	0.01	—	0.85	—	45.42	16.10	0.01	0.11	100.99	0.98	—	—	—	0.01	—
37	37.87	0.02	0.02	—	1.01	0.17	43.35	13.88	—	0.12	96.44	0.98	—	—	—	0.02	—
39	38.12	0.02	—	—	0.53	—	44.32	13.39	—	0.12	96.50	0.99	—	—	—	0.01	—
41	33.81	—	0.05	0.05	1.04	—	42.87	24.01	—	0.14	101.98	0.98	—	—	—	0.02	—
45	38.16	0.01	—	—	1.04	—	43.77	14.04	—	0.14	97.16	0.98	—	—	—	0.02	—
46	38.45	—	0.05	—	0.89	0.10	44.21	14.10	—	0.12	97.91	0.98	—	—	—	0.02	—
47	38.29	0.01	—	—	1.19	0.03	44.60	14.64	—	0.13	98.90	0.98	—	—	—	0.02	—
48	38.44	0.01	0.03	—	1.16	0.13	43.92	15.96	—	0.14	99.77	0.98	—	—	—	0.02	—
49	38.18	—	—	—	0.98	0.05	44.56	13.91	—	0.13	97.81	0.98	—	—	—	0.02	—
50	38.69	—	0.01	—	0.76	—	44.16	13.93	—	0.12	97.66	0.99	—	—	—	0.01	—
164-996D-5X-CC, 20-21 cm:																	
10	38.33	0.02	—	—	0.76	0.03	44.13	12.94	0.01	0.15	96.35	0.99	—	—	—	0.01	—
11	38.95	0.02	0.01	0.02	0.88	—	43.02	15.41	—	0.16	98.46	0.98	—	—	—	0.01	—
13	37.08	0.01	—	0.04	0.86	—	42.63	15.28	0.01	0.14	96.05	0.98	—	—	—	0.02	—
14	38.15	0.02	0.10	0.01	1.13	0.08	43.54	16.21	0.01	0.15	99.39	0.98	—	—	—	0.02	—
15	38.52	—	—	0.01	0.83	0.03	43.98	14.62	—	0.14	98.12	0.98	—	—	—	0.01	—
16	38.87	0.01	—	0.03	0.89	—	44.03	13.25	—	0.12	97.19	0.98	—	—	—	0.02	—
17	38.47	—	0.03	0.01	0.68	—	44.06	14.34	—	0.13	97.74	0.99	—	—	—	0.01	—
18	38.90	0.02	—	—	0.70	—	43.67	14.17	0.01	0.11	97.57	0.99	—	—	—	0.01	—
19	39.01	—	—	0.07	0.70	0.18	43.96	14.24	0.01	0.13	98.28	0.98	—	—	—	0.01	—
20	38.78	—	—	0.04	0.53	0.20	43.74	14.58	0.01	0.13	98.01	0.99	—	—	—	0.01	—

Note: — = below detection limit.

ried in fluids moving upward along a fault above the Blake Ridge Diapir, the $^{87}Sr/^{86}Sr$ values should reflect this deeper pool. At Site 996, however, pore-water Sr values are clearly indistinguishable from measurements of modern (0.709175) and contemporaneous seawater (Farrell et al., 1995). A comparison with Farrell's seawater curve (Fig. 7) also shows that the $^{87}Sr/^{86}Sr$ values of carbonate precipitates recovered throughout the sedimentary section are approximately consistent with the expected $^{87}Sr/^{86}Sr$ composition based on the age of their host sediment. Thus, our data do not indicate an addition of Sr from deep-seated fluids at Site 996.

The Dolomite Nodule

A single dolomite nodule, with a fabric similar to our "type 3" authigenic carbonate (Fig. 3E), was recovered from 51.6 mbsf in Hole 996E. Dolomite (composed of 45 mol% Mg) occurs as microcrystalline cement. The isotopic characteristics of this nodule suggest an origin distinct from the rest of the authigenic carbonates in this section. The $\delta^{13}C$ values of the dolomite nodule (–13.1‰ to –19.2‰) are significantly more enriched in ^{13}C than those of authigenic aragonite recovered elsewhere in the sedimentary section. Furthermore, the $\delta^{18}O$ values (4.8‰–5.4‰) indicate a temperature of formation significantly higher (18°–24°C, using the $\delta^{18}O$/temperature relation of Northrop and Clayton [1966]), than those of the other authigenic carbonates at this site. Although we could assume that the dolomite nodule formed from ^{18}O-depleted water (estimated to be –4.0‰ to –4.5‰ standard mean ocean water [SMOW], based on Northrop and Clayton, [1966]), oxygen isotope measurements of pore water at Site 996 (Egeberg, Chap. 22, this volume) do not indicate such light $\delta^{18}O$ values.

Although authigenic dolomites have been described from various vent locations (e.g., Matsumoto, 1990; Jørgensen, 1992; Kopf et al., 1995), we do not know at this point if the dolomite nodule at Site 996 is directly related to the venting process. The isotopic similarity of the nodule to dolomite found elsewhere on the Blake Ridge at Sites 994, 995, and 997 (Rodriguez et al., Chap. 30, this volume), and the fact that it is the only sample of its kind at Site 996, suggests an origin independent of fluid venting.

$CaCO_3$ Precipitation at Site 996

Our data indicate that precipitation of authigenic carbonates at this site took place at (or near) the seafloor and that continued carbonate formation with increasing sediment depth has not occurred. This inference is supported by the observation that precipitates do not show any significant petrographic or mineralogical changes with depth and that aragonite is the primary authigenic carbonate at Site 996. In addition, both microscopy and electron microprobe analysis do not provide evidence for multistage cementation or changes in the mineral chemistry with depth (mineralogical changes would be expected if nodules grew, or continued to grow, at several depth intervals). Furthermore, $\delta^{13}C$ values of the authigenic carbonates (–30.5‰ to –48.4‰) are similar to the carbon isotopic composition of pore water ΣCO_2 at shallow depth (–28‰ to –45‰). At greater depths, $\delta^{13}C$ values of ΣCO_2 become progressively ^{13}C enriched (+10.5‰ at 43 mbsf), demonstrating that the authigenic carbonates could not have

Table 3. Stable carbon and oxygen isotopic composition of Site 996 carbonate precipitates and sediments.

Core, section, interval (cm)	Depth (mbsf)	Isotopic composition (‰ PDB)		
		Type	$\delta^{13}C$	$\delta^{18}O$
164-996A-				
1H-1, 4-6	0.04	C	–41.37	3.87
1H-1, 21-23	0.21	C	–41.03	3.72
1H-1, 32-34	0.32	C	–44.18	3.84
1H-1, 52-54	0.52	C	–43.01	3.98
1H-1, 63-65	0.63	C	–45.20	3.92
1H-1, 72-74	0.72	C	–42.53	3.62
1H-1, 85-95	0.85	C	–40.43	3.43
1H-1, 85-95	0.85	S	–33.36	2.69
1H-2, 15-16	1.05	C	–48.18	3.91
1H-2, 39-41	1.29	C	–46.75	3.73
1H-2, 56-58	1.46	C	–41.04	3.82
1H-6, 33-38	3.62	S	–13.02	1.73
2H-CC, 14-16	9.13	C	–38.91	4.01
3X-1, 50-52	10.00	C	–36.18	4.44
3X-1, 61-71	10.11	S	–8.42	1.90
8H-2, 0-12	49.61	S	–0.98	0.47
9H-3, 87-102	61.55	S	–3.47	0.47
164-996B-				
1H-1, 0-5	0.00	C	–41.25	3.98
1H-1, 0-5	0.00	C	–42.40	3.81
1H-1, 5-7	0.05	C	–43.59	3.96
1H-1, 35-37	0.35	C	–40.25	3.48
1H-1, 37-39	0.37	C	–43.92	3.70
1H-1, 85-87	0.85	C	–41.42	3.69
1H-3, 135-150	2.44	S	–13.88	1.78
164-996C-				
1H-1, 51-53	0.51	C	–40.54	4.10
1H-1, 56-58	0.56	C	–38.11	4.05
1H-1, 63-65	0.63	C	–41.44	4.12
1H-1, 70-72	0.70	C	–35.48	4.03
1H-1, 108-114	1.08	C	–45.34	3.46
1H-1, 108-114	1.08	S	–22.60	2.04
1H-2, 67-77	1.81	C	–37.92	2.98
1H-2, 67-77	1.81	S	–23.73	2.03
1H-3, 29-31	2.20	C	–44.31	3.84
2H-CC, 0-2	2.40	C	–37.43	3.19
2H-CC, 3-5	2.43	C	–35.78	3.79
164-996D-				
1H-CC, 0-20	0.00	S	–16.98	1.83
1H-CC, 20-40	0.20	C	–30.47	4.10
1H-CC, 20-40	0.20	S	–25.69	2.96
3X-CC, 9-11	13.09	C	–37.60	4.59
4H-6, 135-150	28.59	S	–12.90	0.63
5X-CC, 7-9	32.17	C	–40.90	4.28
5X-CC, 7-9	32.17	C	–45.45	4.48
5X-CC, 7-9	32.17	C	–42.05	4.35
5X-CC, 23-25	32.33	C	–41.25	4.33
6H-2, 52-67	42.99	S	–0.86	0.66
164-996E-				
1H-3, 72-87	3.72	S	–0.35	0.41
2H-1, 137-144	5.45	S	–1.78	0.23
2H-1, 144-150	5.52	S	–1.40	0.16
2H-2, 135-150	6.95	S	–9.34	1.31
2H-4, 134-150	9.94	S	–5.32	0.67
3X-CC, 0-7	13.60	C	–40.40	4.30
3X-CC, 8-12	13.68	C	–33.91	4.34
3X-CC, 21-25	13.81	C	–33.28	4.05
4H-5, 135-150	29.05	S	–0.54	0.21
6X-6, 135-150	50.86	S	–2.36	0.77
6X-CC, 11-13	51.62	C	–16.61	3.13

Note: C = carbonate nodule, S = sediment.

formed in equilibrium with bicarbonate at ambient depth. If these observations can be extrapolated to other vent sites, precipitation of authigenic carbonate at vent sites takes place only at or near the sediment/water interface, and the fluid conduit itself will not be distinctly marked. This means that only the seafloor expression of vent sites will be preserved (as carbonate crusts) and that fossil fluid conduits will be difficult to find in the sedimentary record.

The occurrence of authigenic carbonates at several depth horizons, therefore, can be used to estimate the duration, and lateral shifting, of fluid venting above the Blake Ridge Diapir. Given that the deepest aragonite nodule was recovered from about 30 mbsf, and assuming a constant sedimentation rate of ~48 m/m.y. (Paull, Matsumoto, Wallace, et al., 1996), we can infer that seepage has been going on in this area for at least 600,000 yr. Variations in the oxygen isotopic composition (which might be related to glacial and interglacial periods) support this inference.

CONCLUSIONS

Carbonate precipitates that were recovered from several depth intervals from sediments overlying the Blake Ridge Diapir are dominated by authigenic aragonite cements. Oversaturation of the pore water with respect to aragonite is provided by anaerobic methane oxidation that causes $CaCO_3$ precipitation. The methane flux, which is required to sustain these reactions, is most likely driven by the decomposition of methane hydrates above the diapir and seems to be concentrated along fluid conduits that were observed in the form of vertical, gas hydrate–cemented veins in the sediment.

A comparison of the $\delta^{13}C$ values of carbonate cements to the isotopic composition of the carbon pool indicates that the carbonate nodules derived their carbon from a ^{13}C-depleted ΣCO_2 pool at shallow depth. The oxygen isotopic composition of the carbonate nodules indicates precipitation in, or near, isotopic equilibrium with the regional bottom water. Variations of the $\delta^{18}O$ values with depth might be related to changes in bottom-water conditions over time. The $^{87}Sr/^{86}Sr$ ratios of carbonate precipitates and pore-water samples from Site 996 are indistinguishable from contemporaneous seawater, indicating a shallow Sr source.

Based on these data, the authigenic carbonates at Site 996 seem to have formed at or near the sediment/water interface from a ^{13}C-depleted carbon pool that is fueled by anaerobic methane oxidation (with methane released by the decomposition of gas hydrates below). Furthermore, there is no indication for ongoing carbonate precipitation with depth. This suggests that these near-surface carbonate deposits are the only preservable expression of fluid venting. Thus, on the basis of the depth distribution of the precipitates, fluid venting has been occurring above the Blake Ridge Diapir for at least 600,000 yr.

ACKNOWLEDGMENTS

The authors are thankful to Jutta Heinze and Barbara Valbonesi for their support with sample preparation and XRD analyses. Petra Gloer assisted with electron microprobe measurements at GEOMAR. Isotope analyses were handled very capably by Michael Joachimski at the Geological Institute Erlangen (C and O) and Paul Fullagar at UNC (Sr). We would also like to thank William Showers at North Carolina State University for use of his stable isotope laboratory for sample preparation and analysis. We are grateful for the comments provided by Ryo Matsumoto and Yutaka Yanagimoto, which improved the manuscript. Financial support for this work was provided by the Deutsche Forschungsgemeinschaft (DFG grant Bo 1049/4), and a JOI/USSAC Ocean Drilling Fellowship for NMR.

REFERENCES

Aharon, P., Schwarcz, H.P., and Roberts, H.H., 1997. Radiometric dating of submarine hydrocarbon seeps in the Gulf of Mexico. *Geol. Soc. Am. Bull.*, 109/5:568–579.

Anderson, T.F. and Arthur, M.A., 1983. Stable isotopes of oxygen and carbon and their applications to sedimentologic and paleoenvironmental problems. *In* Arthur, M.A., Anderson, T.F., Kaplan, I.F., Veizer, J., and Land, L.S. (Eds.), *Stable Isotopes in Sedimentary Geology.* SEPM Short Course, 10.

Barry, J.P., Greene, H.G., Orange, D.L., Baxter, C.H., Robinson, B.H., Kochevar, R.E., Nybakken, J.W., Reed, D.L., and McHugh, C.M., 1996. Biologic and geologic characteristics of cold seeps in Monterey Bay, California. *Deep-Sea Res. I*, 43/11–12:1739–1762.

Bohrmann, G., Greinert, J., Suess, E., and Torres, M., 1998. Authigenic carbonates from Cascadia Subduction Zone and their relation to gas hydrate stability. *Geology,* 26/7:647–650.

Borowski, W.S., Paull, C.K., and Ussler, W., III, 1996. Marine pore-water sulfate profiles indicate in situ methane flux from underlying gas hydrate. *Geology,* 24:655–658.

————, 1997. Carbon cycling within the upper methanogenic zone of continental rise sediments: an example from the methane-rich sediments overlying the Blake Ridge fas hydrate deposits. *Mar. Chem.,* 57:299–311.

Brooks, J.M., Field, M.E., and Kennicutt, M.C., II, 1991. Observations of gas hydrates in marine sediments, offshore Northern California. *Mar. Geol.,* 96:103–108.

Burton, E.A., 1993. Controls on marine carbonate cement mineralogy: review and reassessment. *Chem. Geol.,* 105:163–179.

Burton, E.A., and Walter, L.M., 1987. Relative precipitation rate of aragonite and Mg calcite from seawater: temperature or carbonate ion control? *Geology,* 15:111–114.

Carson, B., Westbrook, G.K., Musgrave, R.J., and Suess, E. (Eds.), 1995. *Proc. ODP, Sci. Results,* 146 (Pt 1): College Station, TX (Ocean Drilling Program).

Dillon, W.P., Popenoe, P., Grow, J.A., Klitgord, K.D., Swift, B.A., Paull, C.K., and Cashman, K.V., 1982. Growth faulting and salt diapirism: their relationship and control in the Carolina Trough, Eastern North America. *In* Watkins, J.S., and Drake, C.L. (Eds.), *Studies of Continental Margin Geology.* AAPG Mem., 34:21–46.

Elderfield, H., 1986. Strontium isotope stratigraphy. *Palaeogeogr., Palaeoclimatol., Palaeoecol.,* 57:71–90.

Farrell, J.W., Clemens, S.C., and Gromet, L.P., 1995. Improved chronostratigraphic reference curve of late Neogene seawater $^{87}Sr/^{86}Sr$. *Geology,* 23:403–406.

Goldsmith, J.R., Graf, D.L., and Heard, H.C., 1961. Lattice constants of the calcium-magnesium carbonates. *Am. Mineral.,* 46:453–457.

Greinert, J., in press. Rezente submarine Mineralbildungen: Abbild geochemischer Prozesse an aktiven Fluidaustrittstellen im Aleuten- und Cascadia-Akkretionskomplex. *GEOMAR Rep*.

Hess, J., Bender, M.L., and Schilling, J.G., 1986. Evolution of the ratio of strontium-87 to strontium-86 in seawater from Cretaceous to Present. *Science,* 231:979–984.

Hovland, M., 1992. Hydrocarbon seeps in northern marine waters; their occurrence and effects. *In* Beauchamp, B., von Bitter, P. (Eds.), *Chemosynthesis: Geological Processes and Products*, Soc. Econ. Paleontol. Mineral., 376–382.

Hovland, M., Talbot, M.R., Qvale, H., Olaussen, S., and Aasberg, L., 1987. Methane-related carbonate cements in pockmarks of the North Sea. *J. Sediment. Petrol.,* 57:881–892.

Hudson, J.C., and Anderson, T.F., 1989. Ocean temperatures and isotopic compositions through time. *In* Clarkson, E.N.K., Curry, G.B., and Rolfe, W.D.I. (Eds.), *Environments and Physiology of Fossil Organisms.* Trans. R. Soc. Edinburgh, Earth Sci., 183–192.

Jørgensen, N.O., 1992. Methane-derived carbonate cementation of marine sediments from the Kattegat, Denmark: geochemical and geological evidence. *Mar. Geol.,* 103:1–13.

Kopf, A., Sample, J.C., Bauer, P., Behrmann, J.H., and Erlenkeuser, H., 1995. Diagenetic carbonates from Cascadia Margin: textures, chemical compositions, and oxygen and carbon stable isotope signatures. *In* Carson, B., Westbrook, G.K., Musgrave, R.J., and Suess, E. (Eds.), *Proc. ODP, Sci. Results,* 146 (Pt 1): College Station, TX (Ocean Drilling Program), 117–136.

Kulm, L.D., Suess, E., Moore, J.C., Carson, B., Lewis, B.T., Ritger, S.D., Kadko, D.C., Thornburg, T.M., Embley, R.W., Rugh, W.D., Massoth, G.J., Langseth, M.G., Cochrane, G.R., and Scamman, R.L., 1986. Oregon subduction zone: venting, fauna, and carbonates. *Science,* 231:561–566.

Le Pichon, X., Kobayashi, K., and Crew, K.-N.S., 1992. Fluid venting activity within the eastern Nankai Trough accretionary wedge: a summary of the 1989 Kaiko-Nankai results. *Earth Planet. Sci. Lett.*, 109:303–318.

Longman, M.W., 1980. Carbonate diagenetic textures from nearsurface diagenetic environments. *AAPG Bull.,* 64:461–487.

Lumsden, D.N., 1979. Error in X-ray diffraction estimates of dolomite in carbonate rocks: causes and cures. *AAPG Bull.*, 63:488.

Matsumoto, R., 1990. Vuggy carbonate crust formed by hydrocarbon seepage on the continental shelf of Baffin Island, northeast Canada. *Geochem. J.,* 24:143–158.

Northrop, D.A., and Clayton, R.N., 1966. Oxygen-isotope fractionations in systems containing dolomite. *J. Geol.,* 74:174–196.

Paull, C.K., Chanton, J.P., Neumann, A.C., Coston, J.A., and Martens, C.S., 1992. Indicators of methane-derived carbonates and chemosynthetic organic carbon deposits: examples from the Florida escarpment. *In* Beauchamp, B., von Bitter, P. (Eds.), *Chemosynthesis: Geological Processes and Products.* Soc. Econ. Paleontol. Mineral., 361–375.

Paull, C.K., and Dillon, W.P., 1981. Appearance and distribution of the gas hydrate reflector in the Blake Ridge region, offshore southeastern United States. *USGS Misc. Field Studies Map,* 1252.

Paull, C.K., Fullagar, P.D., Bralower, T.J., and Röhl, U., 1995a. Seawater ventilation of Mid-Pacific guyots drilled during Leg 143. *In* Winterer, E.L., Sager, W.W., Firth, J.V., and Sinton, J.M. (Eds.), *Proc. ODP, Sci. Results,* 143: College Station, TX (Ocean Drilling Program), 231–241.

Paull, C.K., Hecker, B., Commeau, R., Freeman-Lynde, R.P., Neumann, C., Corso, W.P., Golubic, S., Hook, J.E., Sikes, E., and Curray, J., 1984. Biological communities at the Florida escarpement resemble hydrothermal vent taxa. *Science*, 226:965–967.

Paull, C.K., Matsumoto, R., Wallace, P.J., et al., 1996. *Proc. ODP, Init. Repts.,* 164: College Station, TX (Ocean Drilling Program).

Paull, C.K., and Neumann, A.C., 1987. Continental margin brine seeps: their geological consequences. *Geology*, 15:545–548.

Paull, C.K., Ussler, W., III, Borowski, W.S., and Spiess, F.N., 1995b. Methane-rich plumes on the Carolina continental rise: associations with gas hydrates. *Geology*, 23/1:89–92.

Reeburgh, W.S., 1980. Anaerobic methane oxidation: rate depth distribution in Skan Bay sediments. *Earth Planet. Sci. Lett.,* 47:345–352.

Ritger, S., Carson, B., and Suess, E., 1987. Methane-derived authigenic carbonates formed by subduction-induced pore-water expulsion along the Oregon/Washington margin. *Geol. Soc. Am. Bull.,* 98:147–156.

Roberts, H.H., and Aharon, P., 1994. Hydrocarbon-derived carbonate buildups of the northern Gulf of Mexico continental slope: a review of submersible investigations. *Geo-Mar. Lett.*, 14:135–148.

Rosenbaum, J.M., and Sheppard, S.M.F., 1986. An isotopic study of siderite, dolomite and ankerite at high temperatures. *Geochim. Cosmochim. Acta,* 50:1147–1150.

Sample, J.C., and Reid, M.R., 1998. Contrasting hydrogeologic regimes along strike-slip and thrust faults in the Oregon convergent margin: evidence from the chemistry of syntectonic carbonate cements and veins. *Geol. Soc. Am. Bull.*, 110/1:48–59.

Savard, M.M., Beauchamp, B., and Veizer, J., 1996. Significance of aragonite cements around Cretaceous marine methane seeps. *J. Sediment. Res.*, 66/3:430–438.

Soloviev, V.A., and Ginsburg, G.D., 1997. Water segregation in the course of gas hydrate formation and accumulation in submarine gas-seepage fields. *Mar. Geol.*, 137:59–68.

Suess, E., Carson, B., Ritger, S., Moore, J.C., Jones, M., Kulm, L.D., and Cochrane, G., 1985. Biological communities at vent sites along the subduction zones off Oregon. *In* Jones, M.L. (Ed.), *The Hydrothermal Vents of the Eastern Pacific: An Overview.* Bull. Biol. Soc. Wash., 6:475–484.

Suess, E., and Whiticar, M.J., 1989. Methane-derived CO_2 in pore fluids expelled from the Oregon subduction zone. *Palaeogeogr., Palaeoclimatol., Palaeoecol.,* 71:119–136.

Tucholke, B.E., and Mountain, G.S., 1979. Seismic stratigraphy, lithostratigraphy, and paleosedimentation patterns in the North American Basin. *In* Talwani, M., Hay, W., and Ryan, W.B.F. (Eds.), *Deep Drilling Results in the Atlantic Ocean: Continental Margins and Paleoenvironment.* Am. Geophys. Union, Maurice Ewing Ser., 3:58–86.

Wallmann, K., Linke, P., Suess, E., Bohrmann, G., Sahlig, H., Schlüter, M., Dählmann, A., Lammers, S., Greinert, J., and von Mirbach, N., 1997. Quantifying fluid flow, solute mixing, and biogeochemical turnover at cold vents of the eastern Aleutian subduction zone. *Geochim. Cosmochim. Acta*, 61/24:5209–5219.

Date of initial receipt: 20 April 1998
Date of acceptance: 12 January 1999
Ms 164SR-228

Table 4. Carbon, oxygen, and strontium isotopic composition of microdrilled samples from Site 996 and pore water Sr isotopic composition from Sites 994 to 997.

Core, section, interval (cm)	Depth (mbsf)	C and O isotopes (‰)		Sr isotopes		Comment
		$\delta^{18}O$	$\delta^{13}C$	$^{87}Sr/^{86}Sr$	Standard error (1σ)	
164-996A-						
1H-1, 0-1	0.00			0.709141	0.000008	Chester
1H-1, 21-23	0.21	3.5	–47.2	0.709200	0.000008	
1H-1, 21-23	0.21	3.3	–36.1	0.709172	0.000009	
1H-1, 32-34	0.32	3.8	–44.3			
1H-1, 63-65	0.63	3.9	–42.8			
1H-1, 63-65	0.63	3.6	–44.5			
1H-2, 15-16	1.05	3.6	–44.3			
1H-2, 15-16	1.05	3.5	–41.5			
1H-2, 15-16	1.05	3.7	–44.9			
1H-2, 15-16	1.05	3.8	–48.2			
1H-2, 15-16	1.05	3.8	–48.4			
1H-2, 15-16	1.05	3.6	–46.9			
1H-2, 15-16	1.05	3.7	–47.1			
1H-2, 15-16	1.05	3.7	–45.7			
1H-2, 39-41	1.29	3.6	–43.3			Clast
1H-2, 39-41	1.29	3.5	–48.1	0.70919	0.000007	
1H-2, 56-58	1.46	3.3	–37.2			
1H-2, 56-58	1.46	3.6	–42.0			Clast
1H-2, 56-58	1.46	3.5	–39.6			
3X-1, 50-52	10.00	4.1	–34.2			Clast
3X-1, 50-52	10.00	4.2	–36.6	0.709146	0.000007	
164-996B-						
1H-1, 0-5	0.00	3.6	–41.6			
1H-1, 0-5	0.00	3.6	–42.5			
1H-1, 0-5	0.00	3.6	–41.9			
1H-1, 0-5	0.00	3.8	–41.9			Clast
1H-1, 0-5	0.00	3.7	–42.3			
164-996C-						
1H-1, 0-1	0.00			0.709173	0.000007	Bivalve shell
1H-1, 51-53	0.51	3.9	–41.5	0.709133	0.000007	
1H-1, 70-72	0.70	3.9	–42.8			
2H-CC, 0-2	2.40	3.4	–40.3			
2H-CC, 0-2	2.40	3.5	–41.6			
164-996D-						
3X-CC, 9-11	13.09	4.4	–3.9	0.709085	0.000007	Bivalve shell
3X-CC, 9-11	13.09	4.5	–39.1	0.709206	0.000006	
5X-CC, 7-9	32.17	4.4	–44.8	0.709125	0.000007	Pure aragonite
5X-CC, 7-9	32.17	4.2	–39.1			Pure aragonite
5X-CC, 7-9	32.17	4.3	–44.6	0.709146	0.000008	Pure aragonite
5X-CC, 7-9	32.17			0.709132	0.000008	Pure aragonite
5X-CC, 23-25	32.33	4.2	–43.3			
5X-CC, 23-25	32.33	4.2	–43.1			Clast
5X-CC, 23-25	32.33	4.1	–42.5			Clast
5X-CC, 23-25	32.33	3.9	–42.8			Pure aragonite
164-996E-						
3X-CC, 0-7	13.60	4.2	–45.2			
3X-CC, 0-7	13.60	4.7	–46.0			Aragonite needle
3X-CC, 8-12	13.68	3.7	–37.5			
3X-CC, 8-12	13.68	3.9	–37.8			
3X-CC, 12-15	13.72	3.9	–34.1			
3X-CC, 12-15	13.72	4.6	–36.6			Pure aragonite
3X-CC, 12-15	13.72	4.4	–38.8			Pure aragonite
3X-CC, 12-15	13.72	4.5	–43.5			Pure aragonite
3X-CC, 12-15	13.72	4.2	–40.3			Pure aragonite
3X-CC, 12-15	13.72	4.5	–36.9			Pure aragonite
3X-CC, 21-25	13.81	3.8	–35.8	0.709148	0.000008	
3X-CC, 21-25	13.81	4.5	–45.1	0.709168	0.000008	Pure aragonite
3X-CC, 21-25	13.81	4.4	–42.5			Pure aragonite
3X-CC, 21-25	13.81	4.3	–44.9	0.709163	0.000008	Pure aragonite
3X-CC, 21-25	13.81	4.9	–46.9	0.709181	0.000007	Pure aragonite
6X-CC, 11-13	51.62	4.8	–19.2			Dolomite
6X-CC, 11-13	51.62	5.4	–13.1			Dolomite
164-996A-						
1H-6, 33-38	3.62			0.709174	0.000007	Pore water
3X-1, 61-71	10.11			0.709167	0.000006	Pore water
8H-2, 0-2	49.61			0.709168	0.000006	Pore water
9H-3, 87-102	61.55			0.709154	0.000007	Pore water
164-996E-						
2H-2, 135-150	6.95			0.709130	0.000006	Pore water
6X-6, 135-150	50.86			0.709156	0.000008	Pore water
164-994A-						
1H-5, 140-145	7.40			0.709165	0.000007	Pore water
4H-4, 140-145	31.89			0.709182	0.000006	Pore water
164-994C-						
7H-4, 140-145	57.85			0.709169	0.000006	Pore water
164-995A-						
2H-2, 150-155	4.75			0.709204	0.000005	Pore water
5H-5, 145-150	37.65			0.709180	0.000008	Pore water

Table 4 (continued).

Core, section, interval (cm)	Depth (mbsf)	C and O isotopes (‰) $\delta^{18}O$	C and O isotopes (‰) $\delta^{13}C$	Sr isotopes $^{87}Sr/^{86}Sr$	Sr isotopes Standard error (1σ)	Comment
164-997A-						
2H-2, 140-145	5.80			0.709170	0.000006	Pore water
4H-4, 140-145	27.80			0.709175	0.000007	Pore water
3H-2, 145-150	16.80			0.709145	0.000007	Pore water
9H-2, 145-150	64.30			0.709161	0.000009	Pore water

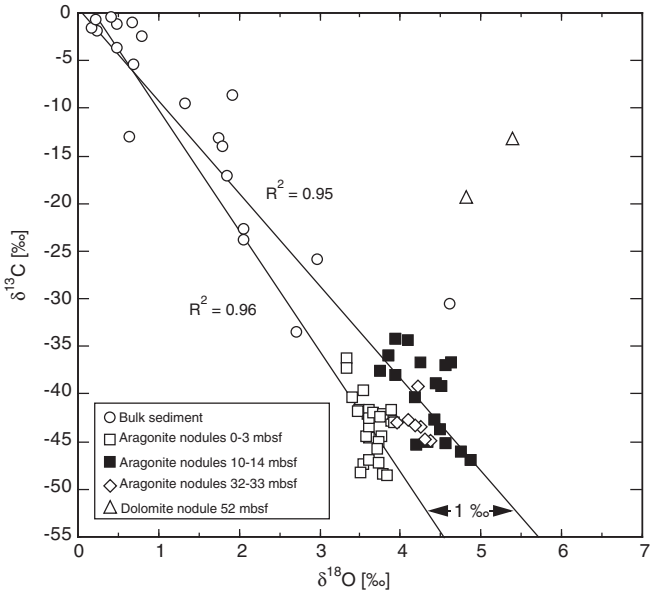

Figure 6. Stable carbon and oxygen isotopic composition of bulk sediment carbonate and carbonate precipitates at Site 996. Note the differences in the oxygen isotopic composition between precipitates from different depth intervals.

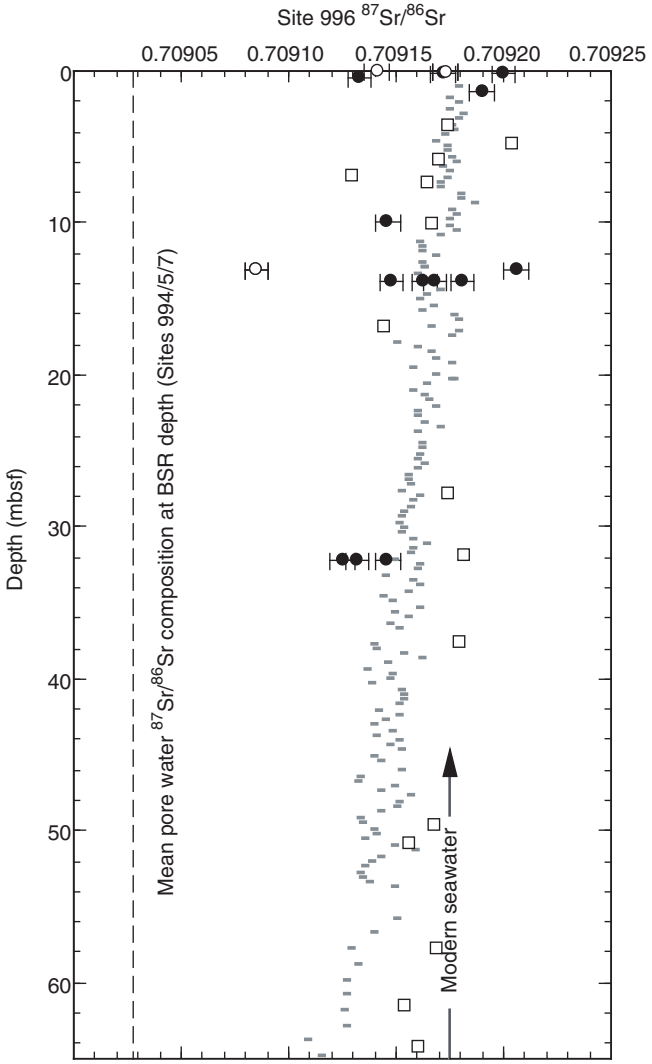

Figure 7. Strontium isotopic composition of aragonite precipitates (solid circles), pore water (squares), and bivalve shells (open circles). Pore-water samples are from Sites 994, 995, 996, and 997. Seawater data (gray bars) are from Farrell et al. (1995). Age model is based on a constant sedimentation rate of 48 m/m.y. See text for discussion.

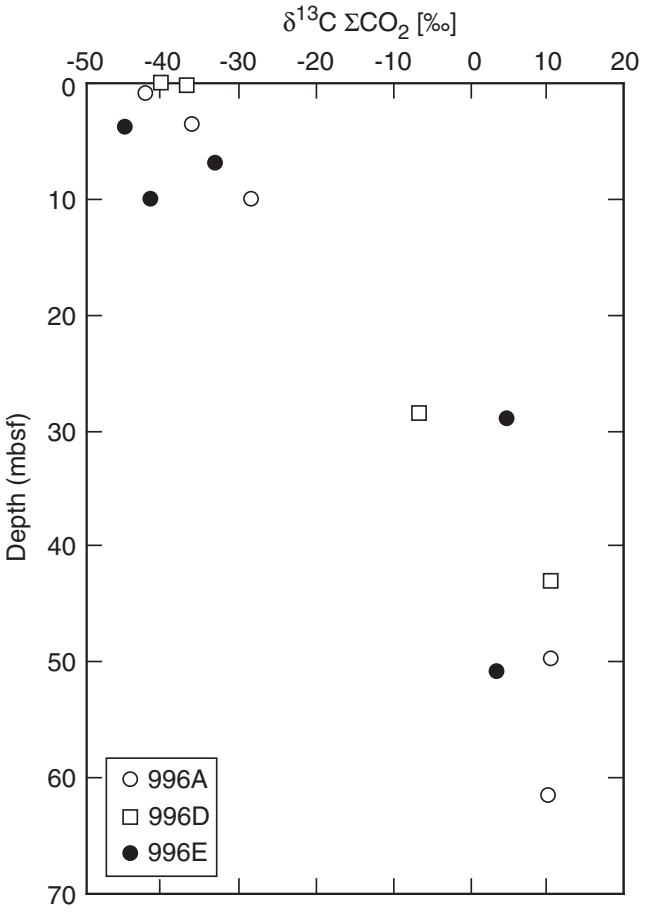

Figure 8. Pore-water ΣCO_2 carbon isotopic composition at Site 996 (Paull et al., Chap. 7, this volume). Note the increase of $\delta^{13}C$ values with depth.

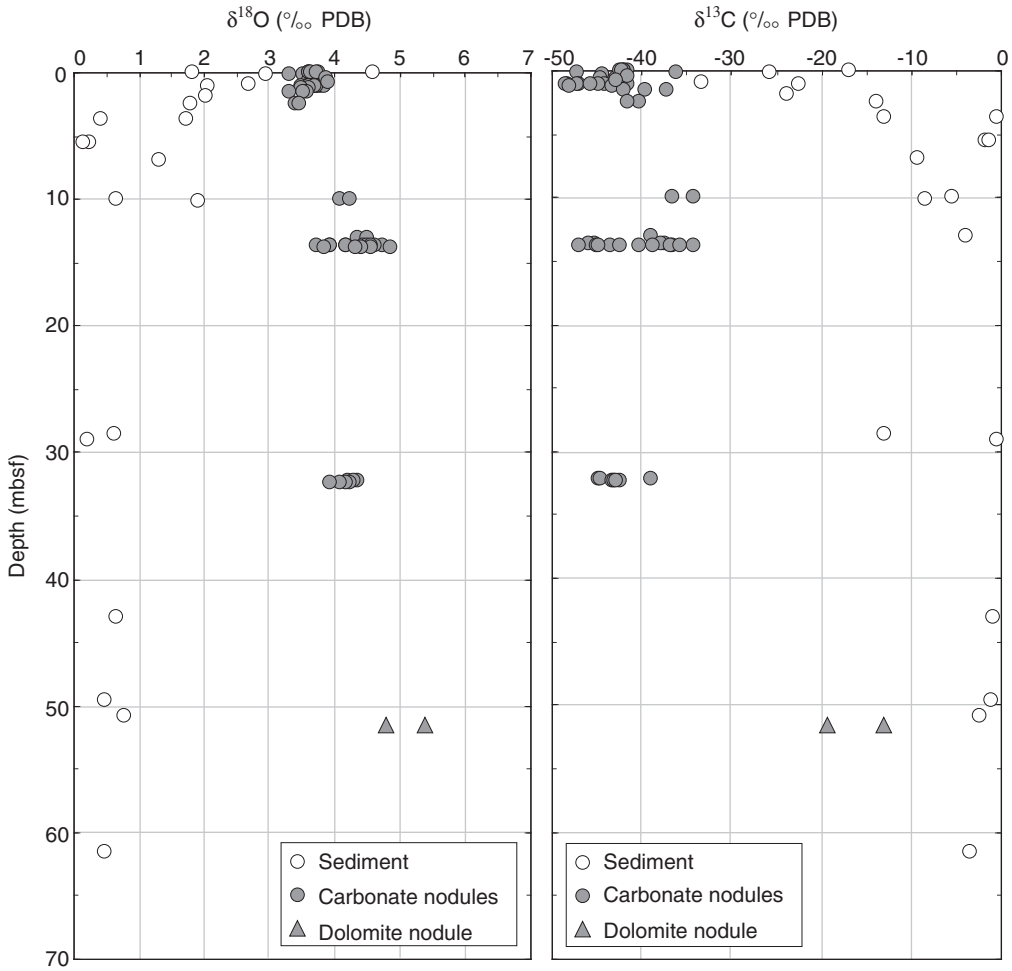

Figure 9. Stable carbon and oxygen isotopic composition of carbonate precipitates (filled circles) and sediment carbonate vs. depth. See text for discussion.

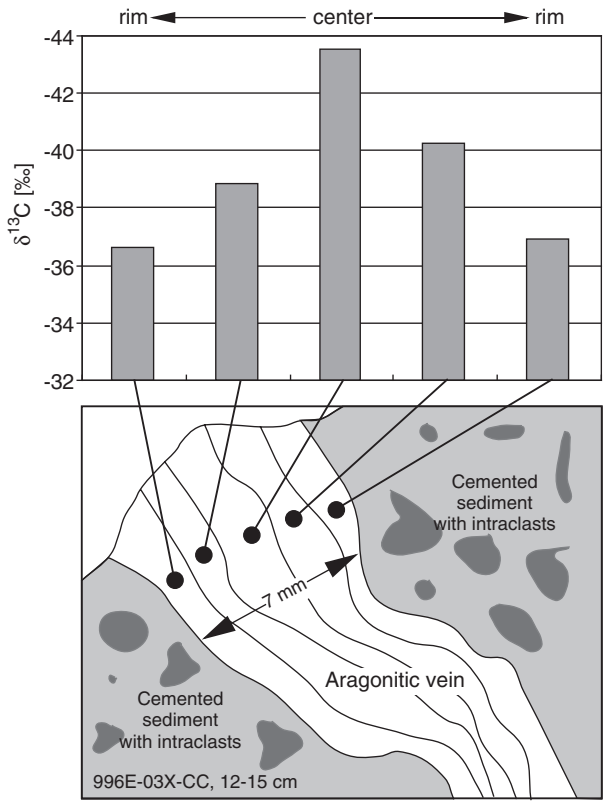

Figure 10. Carbon isotopic composition through an aragonite cemented vein-like void filling within one of the carbonate nodules (Sample 164-996E-3X-CC, 12–15 cm). Diameter of the vein is ~7 mm. The symmetric trend towards more ^{13}C-depleted carbon isotope values from the rim to the center of the vein probably reflects a compositional change of the carbon pool.